Dalton Transactions

Accepted Manuscript

ROYAL SOCIETY OF CHEMISTRY

www.rsc.org/dalton

Cite this: DOI: 10.1039/c0xx00000x

www.rsc.org/xxxxxx

ARTICLE TYPE

Monitoring the Formation of Carbide Crystal Phases during the Thermal Decomposition of 3d Transition Metal Dicarboxylate Complexes

Zachary J. Huba and Everett E. Carpenter*

Received (in XXX, XXX) Xth XXXXXXXXX 20XX, Accepted Xth XXXXXXXXX 20XX
DOI: 10.1039/b000000x

Single molecule precursors can help to simplify the synthesis of complex alloys by minimizing the amount of necessary starting reagents. However, single molecule precursors are time consuming to prepare with very few being commercially available. In this study, a simple precipitation method is used to prepare Fe, Co, and Ni fumarate and succinate complexes. These complexes were then thermally decomposed in an inert atmosphere to test their efficiency as single molecule precursors for the formation of metal carbide phases. Elevated Temperature X-Ray Diffraction was used to identify the crystal phases produced upon decomposition of the metal dicarboxylate complexes. Thermogravimetric Analysis coupled with an infrared detector was used to identify the developed gaseous decomposition products. All complexes tested showed a reduction from the starting M^{2+} oxidation state to the M^0 oxidation state, upon decomposition. Also, each complex tested showed CO_2 and H_2O as gaseous decomposition products. Nickel succinate, iron succinate, and iron fumarate complexes were found to form carbide phases upon decomposition. This proves that transition metal dicarboxylate salts can be employed as efficient single molecule precursors for the formation of metal carbide crystal phases.

Introduction

The metal precursors most commonly employed for the synthesis of metal nanoparticles are low oxidation state metal salts with chloride, nitrate, sulfate, and acetate groups as ligands.[1] These precursors are inexpensive and offer high solubility in a wide variety of polar solvents. To increase solubility in non polar solvents, complexes containing long chained carboxylate ligands (e.g. metal oleate complexes) can be synthesized and used as a metal precursor.[1] By increasing the chain length of the carboxylate ligand, monodispersity and decreased particle sizes can be achieved. Along with long chained carboxylates, organic molecules containing P, S, and Se can be used to complex metal atoms and be used as a precursor to control size and shape.[2] Ligands containing C, N, P, S, and Se can also serve to promote the formation of metal carbides, nitrides, phosphides, sulfides, and selenides from a single molecular precursor.[3-5] One drawback to the use of single molecular precursors is that many are not commercially available, and can be time consuming and expensive to synthesize.[2]

For the synthesis of metal carbides, carbonyl containing complexes are a commonly used single molecule precursor.[6-8] Recently, it has been demonstrated that a cobalt fumarate complex can also be used as an efficient precursor for the synthesis of cobalt carbide nanoparticles.[9, 10] In the current report, we prepare Fe, Co, and Ni fumarate and succinate complexes using a simple precipitation technique. The thermal decomposition of Fe, Co, and Ni fumarate and succinate complexes was then investigated in order to develop a better understanding of their decomposition process and to assess their ability to form metal carbide structures.

Experimental

Iron (II) Fumarate 98%, $Co(NO_3)_2$•$6H_2O$ 97.7%, $Ni(NO_3)_2$•$6H_2O$ 98%, and Na_2Succinate•$4H_2O$ 99% were purchased from Alfa Aesar, and used without further purification. $FeCl_2$•$4H_2O$ 99% and Na_2Fumarate 99% were purchased from Sigma Aldrich Co. and used without further purification.

Synthesis of Dicarboxylate Complexes

For the precipitation of the Fe, Co, and Ni fumarate and succinate complexes, $FeCl_2$•$4H_2O$, $Co(NO_3)_2$•$6H_2O$, and $Ni(NO_3)_2$•$6H_2O$ were used as the metal precursor. To start, 0.800 g (5.0 mmol) of Na_2Fumarate or 1.350 g (5.0 mmol) of Na_2Succinate•$4H_2O$ was added to 5 mL of DI H_2O. The solution was then magnetically stirred and heated to 50 °C. In a separate flask, 5.0 mmol of the desired transition metal precursor (Fe, Co, or Ni) was added to 5 mL of DI H_2O, and vortexed until all solids were dissolved. Once the sodium dicarboxylate solution was at 50 °C and all solids dissolved, the transition metal solution was added dropwise to the sodium dicarboxylate solution. The mixed solution was then allowed to react for 15 minutes. In this 15 minute time frame precipitation of the transition metal dicarboxylate complex could be observed. The solution was then allowed to naturally cool to room temperature with continued

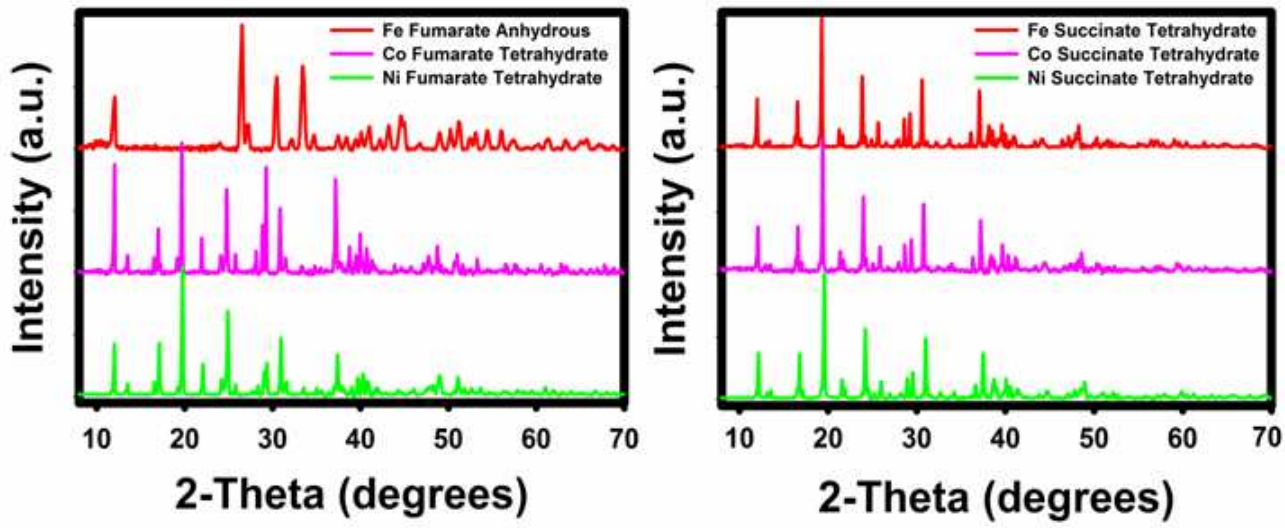

Figure 1. XRD scans of synthesized fumarate (left) and succinate (right) precursor complexes.

stirring. Once at room temperature the solution was centrifuged at 5000 RPM for 5 minutes. After the first centrifugation step, the collected metal dicarboxylate complex was washed with a mixture of 50:50 ethanol and DI H_2O, and centrifuged. This cycle was repeated three times. After washing, the product was allowed to dry in a vacuum oven at room temperature for 48 hours. X-Ray Diffraction patterns for the metal dicarboxylate complexes are shown below in Figure 1; Fourier Transform-Infrared (FT-IR) spectra for the complexes can be found in the Supporting Information (S1).

Elevated Temperature X-Ray Diffraction Analysis (ETXRD)

ETXRD analysis was performed using a Panalytical X'Pert Pro MPD X-Ray Diffractometer (Cu K_α, λ=1.54 Å). Coupled with the diffractometer was an Anton Paar HTK-1200N heating stage with an Anton Paar TCU1000 heating control unit. All metal dicarboxylate complexes were analyzed employing an alumina (Al_2O_3) sample holder, under flowing N_2 atmosphere. The samples were analyzed at temperatures ranging from room temperature to 900 °C. At each temperature, the sample height was adjusted to account for thermal expansion and volume loss due to sample decomposition.

Thermogravimatric analysis coupled with FT-IR detection (TGA-IR)

TGA-IR analysis was conducted under identical conditions for each metal dicarboxylate complex using a Thermal Analysis Q5000 model TGA. Thermograms were collected from room temperature to 600 °C, at a ramp rate of 5 °C/minute. The TGA sample chamber was purged with N_2 gas throughout the analysis at a flow rate of 100 mL/minute. Detection of exhaust gas was conducted with a Thermo Scientific Nicolet 6700 model FT-IR. Exhaust gas was transferred to the FT-IR detector through a stainless steel transfer tube that was heated to 200 °C. The FT-IR detector employed a TGA-FTIR interface stage equipped with a gas flow cell, also heated to 200 °C. FT-IR scans from 500 cm^{-1} to 4000 cm^{-1} were collected every 180 seconds during the TGA analysis. This equates to a scan being collected at 15 °C intervals.

Complimentary Analysis Techniques

Analysis of ETXRD data was performed using XPert Highscore Plus data analysis software. Crystal grain sizes were calculated using Scherrer Ananlysis with instrument broadening determined using a Si wafer. Differential Scanning Calorimetry (DSC) was conducted on a Thermal Analysis DSC Q200 (Supplemental Information). Scans were conducted under N_2 atmosphere, from 25 °C to 600 °C at a ramp rate of 5 °C per minute. Raman spectra were collected on a Thermo Scientific DXR Smart Raman using an excitation wavelength of 532 nm.

Results

The use of metal complexes bearing monobasic carboxylate ligands and their decomposition behaviors has been widely studied.[11,12] However dibasic carboxylate complexes, such as fumarate and succinate complexes, have been studied to a lesser extent. The thermal decomposition of lanthanide, manganese, cobalt, nickel, copper, and zinc fumarates has been previously reported.[13-17] However, most reports were conducted under an air atmosphere, causing the decomposition product formed to be oxide phases. Analysis of the gaseous decomposition products showed CO_2 and H_2O to be produced upon decomposition of the metal organic complexes.[17] The thermal decomposition of manganese fumarate and succinate in a CO_2 atmosphere resulted in the formation of manganese oxide and carbon as the major products.[16] In the present study, the decomposition of Fe, Co, and Ni fumarate and succinate complexes under an N_2 atmosphere resulted in a reduction of the M^{+2} to M^0 particles. Also, for three of the complexes, metal carbide phases were observed.

Cobalt fumarate and cobalt succinate showed very similar decomposition pathways. The first decomposition event was the dehydration of the tetrahydrate complexes. Cobalt succinate lost 30.0 % weight with an onset temperature of 82 °C. Cobalt fumarate lost 29.3 % weight starting at 95 °C. This dehydration was confirmed by the detection of H_2O bending vibrations in collected IR spectra of the gaseous decomposition products

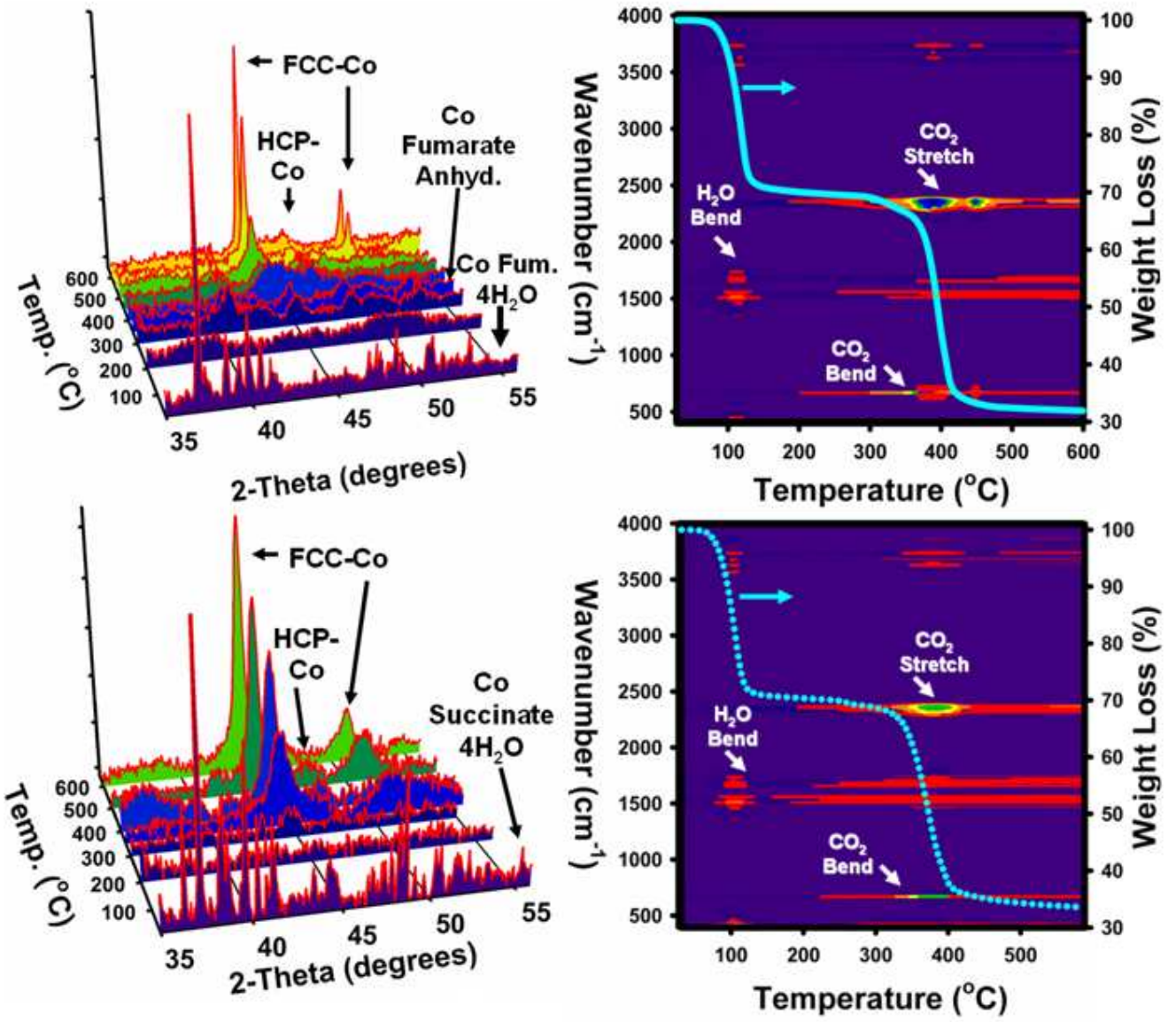

Figure 2. ETXRD scans and TGA-IR contour plots for the decomposition of cobalt fumarate (top) and cobalt succinate (bottom)

(Figure 2). Also, the loss of water resulted in a loss of crystallization in collected ETXRD scans at 200 °C. At 300 °C, cobalt fumarate crystallized into an anhydrous crystal structure, but cobalt succinate showed no significant recrystallization. Increasing temperatures further, caused cobalt fumarate and cobalt succinate complexes to decompose at 378 °C and 349 °C, respectively. The gaseous decomposition products at these temperatures were CO_2 and H_2O. At 400 °C, ETXRD scans showed diffraction intensities consistent with metallic Co phases (face centered cubic (FCC) and hexagonal close packed (HCP)) for cobalt fumarate. Cobalt succinate showed metallic Co phases at 350 °C. Comparing the crystalline products upon decomposition of each cobalt complex, cobalt succinate showed higher intensity and narrower peaks for the Co phases when compared to cobalt fumarate. The average calculated crystal grain sizes for the metallic Co phases at 400 °C were 3.7 nm and 11.6 nm for cobalt fumarate and cobalt succinate, respectively. At temperatures above 400 °C crystal grain sizes increased, along with the disappearance of diffraction intensities corresponding to HCP-Co. Co metal undergoes a martensitic transition from HCP to FCC at temperatures between 400 °C and 500 °C, and helps explain the loss of the hexagonal close packed Co phase at high temperatures.[18]

Nickel fumarate decomposed in a similar manner to the cobalt dicarboxylate complexes. It first showed dehydration at 107 °C, resulting in a 29.2 % weight loss. Decomposition of the nickel fumarate complex occurred at 324 °C and produced CO_2 and H_2O as the gaseous decomposition products. ETXRD showed FCC-Ni to be formed at 350 °C. The crystal grain size for FCC-Ni at 350 °C was calculated to be 3.5 nm. Increasing the temperature to 600 °C only resulted in only slight growth of the FCC-Ni crystals to 7.7 nm. At temperatures above 600 °C, crystal growth occurred more rapidly, resulting in crystal grain sizes of 14.6 nm, 34.8 nm, and 47.2 nm at 700 °C, 800 °C, and 900 °C, respectively.

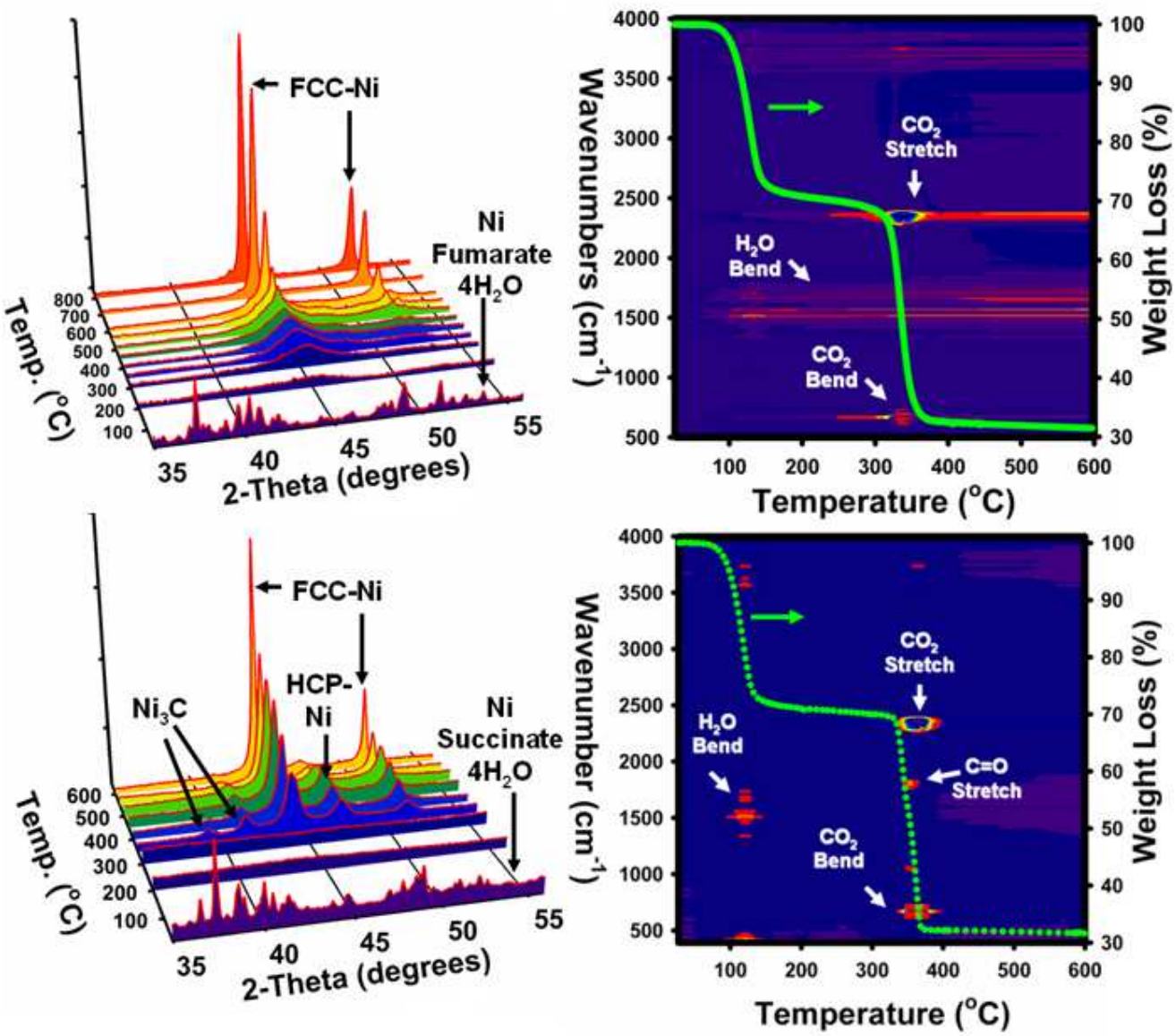

Figure 3. ETXRD scans and TGA-IR contour plots for the decomposition of nickel fumarate (top) and nickel succinate (bottom)

The thermal decomposition of nickel succinate resulted in dramatic differences in decomposition products, when compared to nickel fumarate and cobalt dicarboxylate complexes. Nickel succinate underwent dehydration at 96.6 °C. At 200 °C and 300 °C, no significant diffraction peaks were observed in collected ETXRD scans. The onset of decomposition for the nickel succinate complex occurred at 336 °C, and resulted in 3 crystal phases forming; FCC-Ni, HCP-Ni, and Ni_3C phases were all observed at 350 °C. The formation of Ni_3C does show that dicarboxylate ligands are capable as a carbon source. HCP-Ni is not a thermodynamically stable crystal structure of Ni, and is only observed under conditions with high levels of stress or strain, like those during ion bombardment.[19] Hence, the formation of HCP-Ni could be a strained transition state between the more stable FCC-Ni and Ni_3C phases. At 400 °C only HCP- Ni and FCC-Ni phases were identified, implying the decomposition of the Ni_3C phase. This corresponds well to literature values of Ni_3C decomposition occurring around 400 °C.[20, 21] Above 400 °C, an increase in FCC-Ni composition corresponding to a decrease in HCP-Ni phase was observed.

Iron fumarate was the only dicarboxylate complex investigated that started with an anhydrous hydration state. The lack of coordinated water molecules resulted in no observable events in collected ETXRD and TGA-IR spectra from 25 °C to 350 °C. With an onset temperature of 391 °C, decomposition of the Fe fumarate complex took place, resulting in a weight loss of 48.5% and liberation of CO_2. ETXRD collected at 400 °C showed only weak intensities consistent with the Fe fumarate precursor complex. However, increasing to 450 °C resulted in the observance of 3 phases: FeO, BCC-Fe, and Fe_3C. At 500 °C the FeO was completely reduced, resulting in a crystal phase composition of 42.3% BCC-Fe and 57.3% Fe_3C. The Fe_3C composition further increased to 72.3% at 550 °C but dropped to 29.8% at 600 °C, with the balance phase being BCC-Fe. The apparent decomposition of Fe_3C to BCC-Fe agrees well with a weight loss of 10.73%, beginning at 550 °C. At temperatures

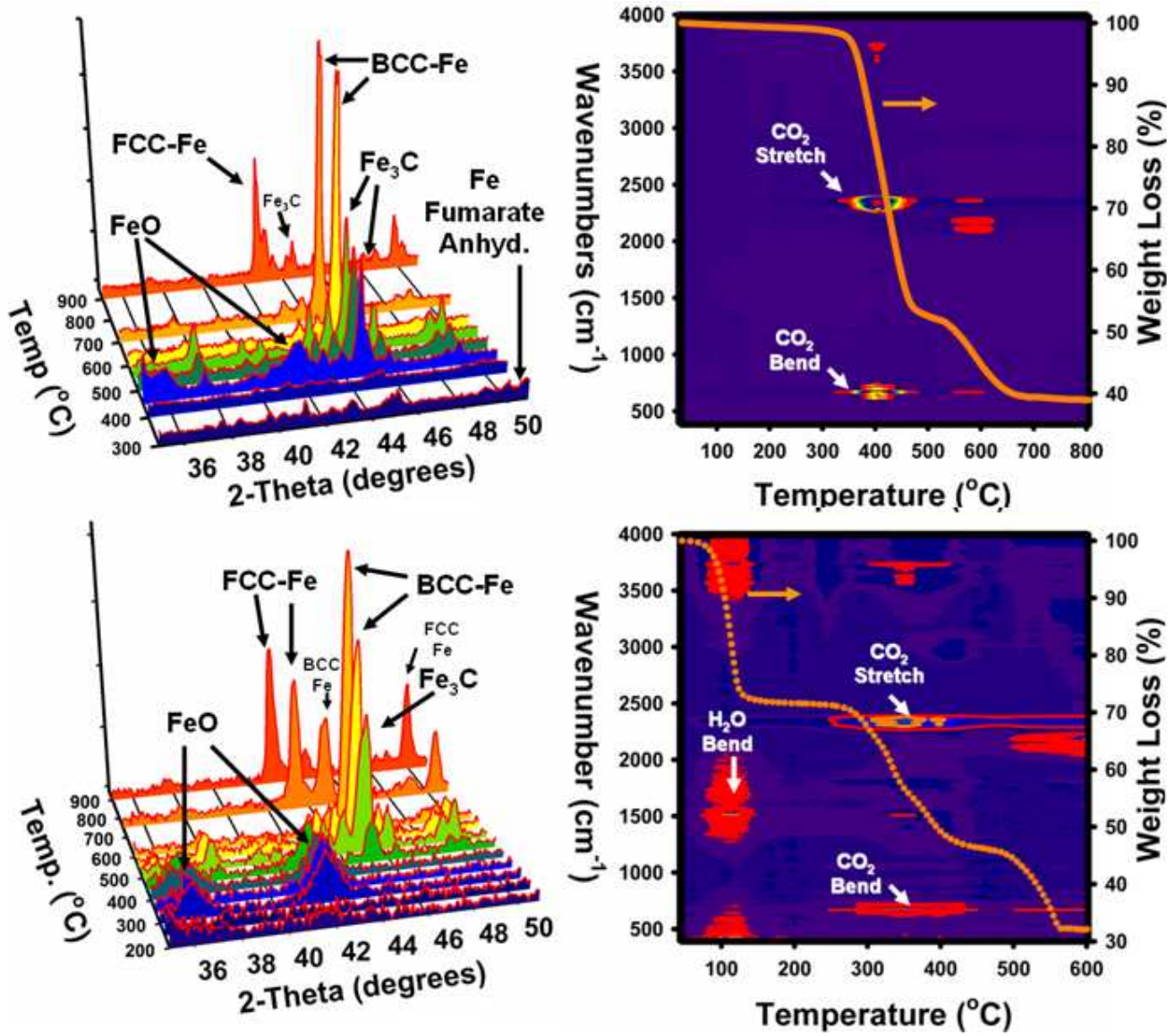

Figure 4. ETXRD scans and TGA-IR contour plots for the decomposition of iron fumarate (top) and iron succinate (bottom)

above 600 °C, BCC-Fe transitioned to FCC-Fe.

Fe Succinate showed a dehydration process beginning at 77.5 °C resulting in a 28.04 % weight loss, similar to all the other tetrahydrate complexes tested. ETXRD scans showed that after the dehydration process, no crystalline components were present until the onset of the decomposition process at 277 °C. The decomposition process led to the liberation of CO_2 and H_2O, and the formation of FeO. FeO was the major crystalline component present in ETXRD scans collected from 300 °C to 450 °C. At 450 °C, peaks consistent with Fe_3C could be observed resulting in a phase composition of 24.1 % Fe_3C and 75.9% FeO. Increasing to 500 °C caused the reduction of the FeO phase, with 30.6% BCC-Fe and 69.4% Fe_3C being present. Increasing temperatures further produced ETXRD results very similar to those observed with Fe fumarate; Fe_3C phase % slowly decreased at the expense of BCC-Fe, with BCC-Fe showing increased crystal grain sizes with increasing temperature. At 750 °C, a mixture of Fe_3C, BCC-Fe, and FCC-Fe was identified, while at 900 °C only FCC-Fe and Fe_3C were observed.

In all complexes analyzed, the observed weight percentages at 600 °C were higher than would be predicted for the decomposition of the metal dicarboxylate complexes into pure metal particles. For example, the decomposition of Co fumarate would be predicted to result in 24% pure Co^0. However, the remaining weight percent observed at 600 °C was 31.92%. Raman Spectroscopy was used to investigate the possible presence of surface carbon residue or amorphous metal oxides. Raman analysis of samples from the ETXRD study resulted in the observance of D and G bands of carbon in collected Raman spectra at 1355 cm^{-1} and 1575 cm^{-1}, respectively. Also a peak at 2330 cm^{-1} was detected in each spectrum which corresponds to the stretching mode of N_2. Most complexes showed no presence of contaminant metal oxides; metal oxides commonly show Raman active modes between 500 cm^{-1} to 800 cm^{-1}.[22] The presence of the D and G bands of carbon shows a significant amount of carbon residue to exist, helping to explain the higher

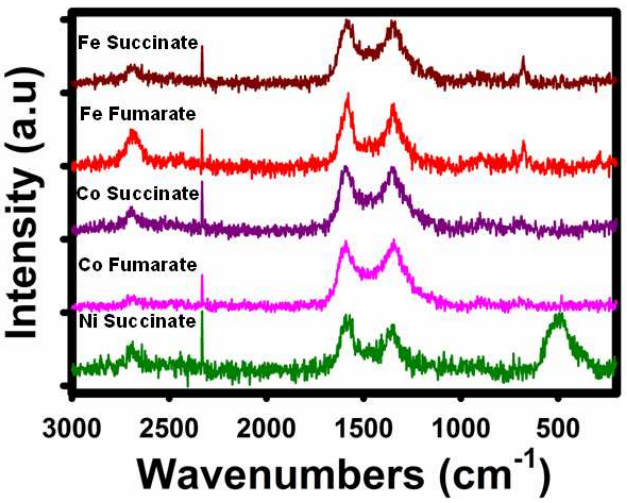

Figure 5. Raman spectra for the metal dicarboxylate complexes heated to 900 °C.

than expected weights resulting from decomposition of the dicarboxylate complexes. D and G band ratios were around 1 for each product tested and implies the resulting carbon structure to be poorly ordered.[23] However, the presence of carbon does substantiate that decomposition of the fumarate and succinate ligands to produce free carbon atoms.

Discussion

From the ETXRD and Raman data, it is shown that the thermal decomposition of all of metal dicarboxylate complexes tested cause a reduction of the M^{2+} atoms to M^0 and led to the formation of amorphous carbon. During the decomposition/reduction process, CO_2 was the major gaseous product observed in TGA-IR studies. No significant signal for C-H, C-C, or C=C stretch was observed for any complex tested, implying that the central ethane and ethylene moieties of the succinate and fumarate ligands are oxidized to CO_2, and serve as a possible reduction source for the metals. Also, ethylene and ethane are commonly used as gaseous carbon sources for metal catalyzed production of ordered carbon structures.[24] Hence, the decomposition of the fumarate and succinate ligands supplies a reduction and carbon source for the formation of metal carbide structures. However, only three of the complexes investigated formed metal carbide crystal phases (Fe fumarate, Fe succinate, and Ni Succinate).

The decomposition of the cobalt complexes showed no crystalline carbide phases. The lack of carbide formation for the tested cobalt complexes can be explained by looking at the decomposition temperatures for the stable Co carbide phases: Co_3C and Co_2C. Co_3C decomposes at 315 °C and Co_2C decomposes at 300 °C.[25] Both cobalt complexes decomposed well above these temperatures, and were energetically favored to form metallic cobalt crystal structures.

While none of the cobalt dicarboxylate complexes decomposed to a carbide phase, Ni succinate formed 15.8 % Ni_3C at 350 °C. Ni_3C has a higher decomposition temperature than the Co_xC phases, falling between 400 °C and 425 °C.[20, 21] Ni succinate and Ni Fumarate decomposed at 336 °C and 324°C, respectively. However only Ni succinate formed Ni_3C and Ni fumarate did not.

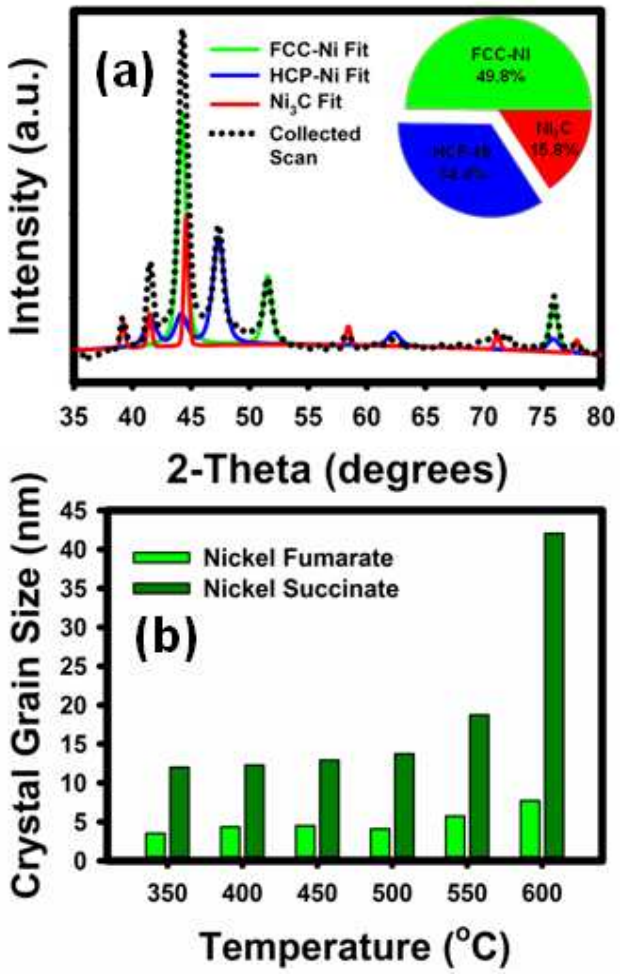

Figure 6. (a) XRD scan taken during the decomposition of Ni succinate at 350 °C. Fits and phase percentages are shown for FCC-Ni, HCP-Ni, and Ni_3C. Lattice parameters, space groups, and Wyckoff positions for each phase can be found in the Electronic Supplementary Information
(b) Average crystal grain sizes as a function of temperature for phases produced from the decomposition of Ni fumarate and Ni succinate.

Analysis of ETXRD scans for the decomposition of both Ni complexes showed dramatic differences in average crystal grain sizes for the crystalline decomposition products of each Ni complex. The crystals phases formed as a result of the decomposition of Ni Fumarate showed significantly smaller crystal grain sizes than Ni Succinate (Figure 6(a)). Carbon solubility in transition metal crystal structures is highly dependent on the crystal grain size; decreasing grain sizes typically show a decrease in carbon solubility.[26] Hence, lower carbon solubility due to small grain sizes for the Ni crystal phase formed upon decomposition of Ni fumarate is one possible explanation for its inability to form the Ni_3C phase.

Both Fe complexes formed carbide phases upon decomposition. However, with increasing temperature the carbide phases decomposed to BCC-Fe. During the heating process, no pure phase Fe_3C was observed. Now to be able to label Fe fumarate or succinate as a true single molecule precursor for Fe_xC phases, a pure phase carbide should be attained. At temperatures above 600 °C, the BCC-Fe phase transitioned to FCC-Fe. FCC-Fe possesses carbon solubility values that are significantly higher than BCC-Fe (on the order of 10 times higher).[27] This difference

in carbon solubility of the two iron crystal phases was exploited to achieve the pure phase Fe_3C. By heating Fe fumarate quickly to 900 °C to form FCC-Fe and then cooling at a rate of 100 °C/min, phase pure Fe_3C can be formed (Figure 7). The phase pure Fe_3C was ferromagnetic in nature at room temperature, possessing a magnetic saturation value of 124 emu/g. This magnetization is lower than a theoretical maximum magnetization of 143 emu/g.[28, 29] This deviation in magnetization can be attributed to the excess carbon as observed in collected Raman spectra. The successful synthesis of phase pure Fe_3C shows that late row 3d transition metal dicarboxylates can act as a single molecule precursor for the synthesis of pure phase metal carbide crystal phases under appropriate synthesis conditions.

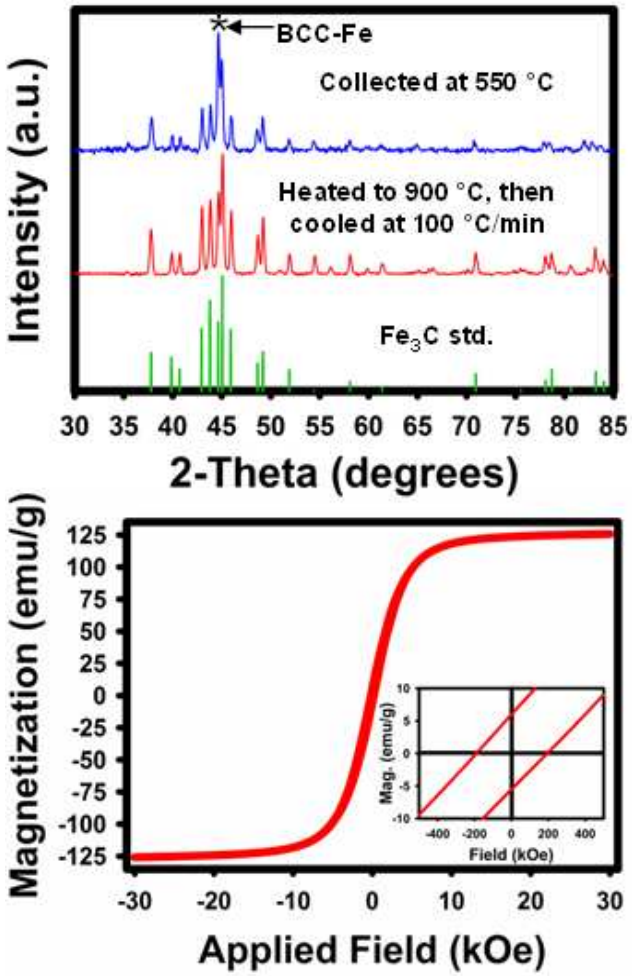

Figure 7. (a) XRD scan of Fe_3C samples as a result of decomposition of Fe dicarboxylate complexes. (b) Magnetization vs. applied field curve for phase pure Fe_3C

Conclusion

The purpose of this investigation was to examine the ability of Fe, Co, and Ni fumarate and succinate complexes to act as single molecule precursors for the synthesis of endothermic carbide phases. In all cases, the decomposition of the metal dicarboxylate complex resulted in a reduction of the M^{2+} precursor to an M^0 state. In three of the complexes, metal carbide phases were observed. Nickel succinate decomposed into a mixture of FCC-Ni, HCP-Ni, and Ni_3C at 350 °C. Fe succinate and Fe fumarate formed Fe_3C at 500 °C and 550 °C, but decomposed to BCC-Fe at higher temperatures. At 550 °C, both iron complexes formed between 60-70 % Fe_3C, with Fe_3C grain sizes of 107 nm for Fe fumarate and 40 nm for Fe succinate. For all complexes, the gaseous decomposition products were CO_2 and H_2O. This report shows that dicarboxylate ligands can serve as carbon sources for the synthesis of endothermic 3d metal carbide crystal phases.

Acknowledgements

Financial support from the ARPA-e REACT program 1574-1674 is greatly acknowledged. The help of the staff of the VCU Nanomaterials Core Characterization Facility is also greatly appreciated. This work was also partially funded through a graduate research fellowship through Altria Group Inc.

Notes and references

* *1001 W. Main Streeet, Richmond, Va 23284, USA; E-mail:ecarpenter2@vcu.edu*

† Electronic Supplementary Information (ESI) available: FT-IR spectra and DSC thermograms for the dicarboxylate complexes. TGA-IR plots of Na fumarate and Na succinate starting materials. Also, the crystallographic parameters for the Ni phases identified in Figure 6. See DOI: 10.1039/b000000x

1. M. A. Willard, L. K. Kurihara, E. E. Carpenter, S. Calvin and V. G. Harris, International Materials Reviews, 2004, 49, 125-170.
2. C. Amiens, B. Chaudret, D. Ciuculescu, V. Colliere, K. Fajerwerg, P. Fau, M. Kahn, A. Maisonnat, K. Soulantica and K. Philippot, New Journal of Chemistry, 2013.
3. J. Park, B. Koo, K. Y. Yoon, Y. Hwang, M. Kang, J. G. Park and T. Hyeon, Journal of the American Chemical Society, 2005, 127, 8433-8440.
4. W. Maneeprakorn, M. A. Malik and P. O'Brien, Journal of Materials Chemistry, 2010, 20, 2329-2335.
5. W. Maneeprakorn, C. Q. Nguyen, M. A. Malik, P. O'Brien and J. Raftery, Dalton Transactions, 2009, 2103-2108.
6. A. Meffre, B. Mehdaoui, V. Kelsen, P. F. Fazzini, J. Carrey, S. Lachaize, M. Respaud and B. Chaudret, Nano Letters, 2012, 12, 4722-4728.
7. M. D. Shultz, S. Calvin, F. Gonzalez-Jimenez, V. Mujica, B. C. Alleluia and E. E. Carpenter, Chemistry of Materials, 2009, 21, 5594-5600.
8. C. Yang, H. B. Zhao, Y. L. Hou and D. Ma, Journal of the American Chemical Society, 2012, 134, 15814-15821.
9. A. A. El-Gendy, T. Almugaiteeb and E. E. Carpenter, Journal of Magnetism and Magnetic Materials, 2013, 348, 136-139.
10. A. A. El-Gendy, M. Qian, Z. J. Huba, S. N. Khanna and E. E. Carpenter, Applied Physics Letters, 2014, 104, -.
11. J. Mu and D. D. Perlmutter, Thermochimica Acta, 1981, 49, 207-218.
12. M. R. Buck, A. J. Biacchi and R. E. Schaak, Chemistry of Materials, 2014, 26, 1492-1499.
13. B. S. Randhawa and M. Kaur, Journal of Thermal Analysis and Calorimetry, 2007, 89, 251-255.
14. P. S. Bassi, B. S. Randhawa, C. M. Khajuria and S. Kaur, Journal of Thermal Analysis, 1987, 32, 569-577.
15. Y. Suzuki, Thermochimica Acta, 1995, 255, 155-170.
16. Y. Suzuki, K. Muraishi and H. Ito, Thermochimica Acta, 1995, 258, 231-241.
17. E. Y. Ionashiro, F. J. Caires, A. B. Siqueira, L. S. Lima and C. T. Carvalho, Journal of Thermal Analysis and Calorimetry, 2012, 108, 1183-1188.
18. F. Frey, W. Prandl, J. Schneider, C. Zeyen and K. Ziebeck, Journal of Physics F-Metal Physics, 1979, 9, 603-616.

19. E. Johnson, T. Wohlenberg and W. A. Grant, Phase Transitions, 1979, 1, 23-33.
20. Y. Leng, L. Xie, F. Liao, J. Zheng and X. Li, Thermochimica Acta, 2008, 473, 14-18.
21. Z. L. Schaefer, K. M. Weeber, R. Misra, P. Schiffer and R. E. Schaak, Chemistry of Materials, 2011, 23, 2475-2480.
22. C. W. Tang, C. B. Wang and S. H. Chien, Thermochimica Acta, 2008, 473, 68-73.
23. A. C. Ferrari and J. Robertson, Physical Review B, 2000, 61, 14095-14107.
24. C. Park and R. T. K. Baker, J. Catal., 1998, 179, 361-374.
25. K. J. Carroll, Z. J. Huba, S. R. Spurgeon, M. Qian, S. N. Khanna, D. M. Hudgins, M. L. Taheri and E. E. Carpenter, Applied Physics Letters, 2012, 101, 012409.
26. P. A. Chernavskii, V. I. Zaikovskii and G. V. Pankina, Russ. J. Phys. Chem. A, 2012, 86, 1274-1280.
27. D. E. Jiang and E. A. Carter, Physical Review B, 2003, 67.
28. J. M. D. Coey, Cambridge University Press, Editon edn., 2010.
29. J. M. D. Coey, IEEE Transactions on Magnetics, 2011, 47, 4671-4681.

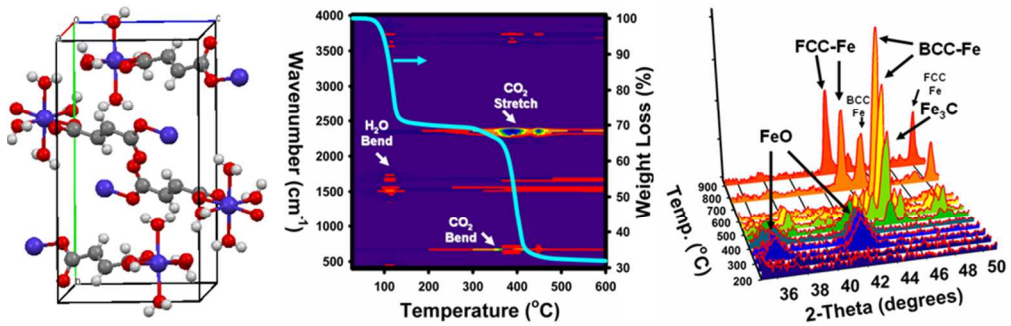

252x80mm (96 x 96 DPI)